Measurements of cross sections and oscillator strengths for Ne by electron-energy-loss spectroscopy

T. Y. Suzuki, H. Suzuki, and S. Ohtani
Institute for Laser Science, University of Electro-Communications, Chofugaoka 1-5-1, Chofu-Shi, Tokyo 182 Japan

B. S. Min, T. Takayanagi, and K. Wakiya
Department of Physics, Sophia University, Kioicho 7-1, Chiyoda-ku, Tokyo 102 Japan

(Received 18 February 1994)

Differential cross sections and generalized oscillator strengths have been measured for two optically allowed transitions $2p^6(^1S_0)\rightarrow 2p^5(^2P_{1/2,3/2})3s$ and the optically forbidden transition $2p^6(^1S_0)\rightarrow 2p^5(^2P_{1/2})3p$ in Ne. These measurements are carried out for electron kinetic energies 300, 400, and 500 eV at small scattering angles ($\theta=2.4°-33.7°$) by means of electron-energy-loss spectroscopy. Optical oscillator strengths have been determined by extrapolating the generalized oscillator strengths to zero momentum transfer, as (0.137±0.018) and (0.0106±0.0014), for the $2p^5(^2P_{1/2})3s$ and $2p^5(^2P_{3/2})3s$ states, respectively. Integrated cross sections have been calculated by integrating the differential cross sections for each impact energy. The errrors are estimated to be less than 13%.

PACS number(s): 34.80.Dp

I. INTRODUCTION

We have performed a series of measurements of differential cross sections (DCS's) and generalized oscillator strengths (GOS's) for the electron-impact excitation of the resonance lines in rare-gas atoms up to now. As the final report of this series, we present the cross sections and oscillator strengths for Ne in the present paper. The results of measurements for resonance lines in Ar, Kr, and Xe have already been published [1–3].

Relatively plentiful theoretical calculations are available for electron-impact inelastic scattering in Ne. Ganas and Green [4] reported the calculations of the GOS's and the integrated cross sections (ICS's) by the Born approximation based on the analytic atomic independent-particle model. By the distorted Born approximation, Sawada, Purcell, and Green [5] reported the GOS's and ICS's using the same model as those of Ganas and Green in order to study the effects of distortion as well as exchange contributions in lower-energy regions. Machado, Leal, and Csanak [6] reported the calculations of the DCS's and ICS's for electron-impact excitation of all the $3s, 3s'$ levels, and certain of the $3p, 3p'$ levels of Ne using the first-order, many-body theory (FOMBT).

In respect to experimental studies, the inelastic DCS's and ICS's were given by 25, 30, 50, and 100 eV impact energies by Register *et al.* [7]. Phillips, Anderson, and Lin [8] reported apparent and direct excitation cross sections for the four $2p^5 3s$ levels using a laser-induced fluorescence technique from the threshold to 300 eV impact energy. Shaw, Borge, and Campos [9] reported the emission cross sections from the $2p^5 np$ states, which are designated as $np'[1/2]_0$ ($n=3,4,5$) in the *Jl* coupling notation, by electron impact. The electron-impact energy range was from the threshold to 400 eV.

In the present work, the DCS's and the GOS's for the $2p^5(^2P_{1/2,3/2})3s$ and $2p^5(^2P_{1/2})3p$ states, which are designated as $3s'[1/2]^0_1$, $3s[3/2]^0_1$, and $3p'[1/2]_0$ according to the *Jl* coupling notation [10], respectively, are determined at 300, 400, and 500 eV impact energies by means of electron-energy-loss spectroscopy (EELS). These states are designated as the $1s_2$, $1s_4$, and $2p_1$ states in Paschen's notation, in the same order. Because of its simplicity and tradition in Ne, we will use Paschen's notation for the excited states in Ne in this paper. The optical oscillator strengths (OOS's) and ICS's are also deduced from the GOS's and are compared with the results of other measurements and calculations.

II. EXPERIMENTAL PROCEDURES

Details of the experimental apparatus have been described in the preceding papers [1–3]. The apparatus consists of an electron gun, an electron-energy selector, a target source, and an electron energy analyzer. All of these components are enclosed in a vacuum chamber (1×10^{-7} Torr). In this measurement, typical energy resolution of the apparatus is 50 meV full width at half maximum (FWHM). The angular resolution which was estimated from measurements of the angular distribution of the primary electron beam is 0.4° (FWHM).

Absolute DCS's are given from the relation

$$\left[\frac{d\sigma}{d\Omega}\right]_{\text{inel}} \Big/ \left[\frac{d\sigma}{d\Omega}\right]_{\text{el}} = I_{\text{inel}}/I_{\text{el}} , \tag{1}$$

where I is the scattering intensity that is given by the corresponding peak area of the energy-loss spectra. The suffixes "inel" and "el" denote inelastic and elastic scattering, respectively. The actual zero-scattering angle has been calibrated using the symmetry nature of the intensity ratio $I_{\text{inel}}/I_{\text{el}}$ around 0°. The $(d\sigma/d\Omega)_{\text{el}}$ were obtained by a calculation using a fitting function, which was based on the data of the absolute elastic-scattering cross

sections measured by Bromberg [11] and Jansen *et al.* [12] and calculated by Byron and Joachain [13]. Using Eq. (1), the $(d\sigma/d\Omega)_{\text{inel}}$ can be determined by multiplying the ratio with the $(d\sigma/d\Omega)_{\text{el}}$.

The GOS $F(K)$ is calculated from the following equation [14]:

$$F(K)=\frac{W}{2}\frac{k_i}{k_f}K^2\left[\frac{d\sigma}{d\Omega}\right], \tag{2}$$

where W is the excitation energy, k_i and k_f are the momenta of the colliding electrons before and after the collision, and K is the absolute value of the momentum-transfer vector. All quantities are in atomic units. The limit of the GOS at $K^2=0$ gives the OOS whether the Born approximation is valid or not. In order to extrapolate the experimental results to zero momentum transfer, when the Born approximation holds, we have fitted the GOS values using the least-squares method with the polynomials of the form [15]

$$F(K)=\frac{1}{(1+x^2)^6}\left[f_0+\sum_{n=1}^{m}f_n\left[\frac{x^2}{1+x^2}\right]^n\right], \tag{3}$$

where f_0 is the OOS, f_n are the coefficients, x is equal to K/Y, and Y is equal to $\sqrt{2I}+\sqrt{2(I-W)}$, while I and W are the ionization and excitation energy, respectively. When the Born approximation is not valid, the GOS values for optically forbidden transitions have been fitted with the polynomials of the following form [16]:

$$f(K,E_i)=\frac{x^2}{(1+x^2)^2}\sum_{n=0}^{m}c_n\left[\frac{x}{(1+x^2)^{1/2}}\right]^n, \tag{4}$$

where c_n are the coefficients and x is the same as those in Eq. (3).

By employing both Eqs. (2) and (3), the ICS σ is obtained as follows:

$$\sigma=\frac{4\pi}{Wk_i^2}\int_{k_i-k_f}^{k_i+k_f}\frac{F(K)}{K}dK\ . \tag{5}$$

We make the numerical calculations of the ICS in the Born approximation according to this formula.

III. RESULTS AND DISCUSSION

A typical energy-loss spectrum is shown in Fig. 1, which is taken at the impact energy of 500 eV and a scattering angle of 5°. The energy-loss peaks have been identified by comparing them with the spectroscopic data of the transition energies from the table compiled by Moore [10].

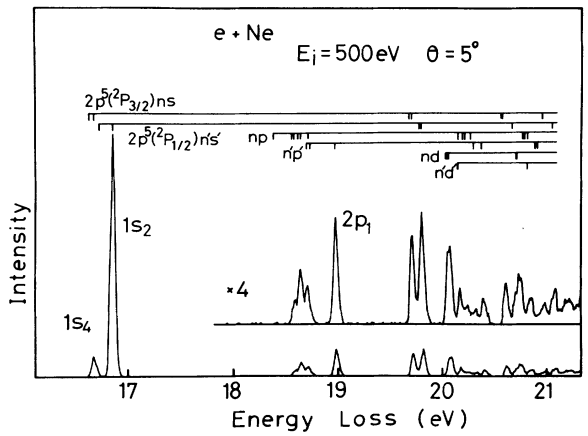

FIG. 1. A typical electron-energy-loss spectrum of Ne for the impact energy 500 eV at the scattering angle 5°.

The most intense peak at 16.848 eV corresponds to the excitation to the $2p^5(^2P_{1/2})3s$ state ($1s_2$ in the Paschen's notation) from the ground state, an adjacent peak at 16.671 eV corresponds to the excitation to the $2p^5(^2P_{3/2})3s$ ($1s_4$ in Paschen's notation), and a peak at 18.966 eV corresponds to the $2p^5(^2P_{1/2})3p$ ($2p_1$ in Paschen's notation) excitation. The intensity ratios of the $1s_2$, $1s_4$, and $2p_1$ peaks to the elastic-scattering peak are given in Table I.

The absolute elastic-scattering cross sections are obtained using a fitting function, which is normalized to the zero-angle cross section calculated by Byron and Joachain [13], on the basis of those measured by Bromberg [11] and Jansen *et al.* [12]. It is known that a curve of a semilogarithmic plot of $(d\sigma/d\Omega)_{\text{el}}$ against K shows a linear behavior in the region of small K [12]. The elastic-scattering cross sections are fitted to a formula as follows:

$$\ln\left[\frac{d\sigma}{d\Omega}\right]_{\text{el}}=c_0+c_1K+c_2K^2+c_3K^3\ , \tag{6}$$

where c_0, c_1, c_2, and c_3 are the fitting parameters. Numerical results of $(d\sigma/d\Omega)_{\text{el}}$ are listed in Table I.

The DCS's for the $1s_2$ and $1s_4$ excitation for the impact energies 300, 400, and 500 eV are shown in Fig. 2 as functions of the scattering angle in the region lower than

TABLE I. The intensity ratios $(d\sigma/d\Omega)_{\text{inel}}/(d\sigma/d\Omega)_{\text{el}}$ and the DCS's $[d\sigma/d\Omega]_{\text{inel}}$ (in atomic units) for excitation of the $1s_2$, $1s_4$, and $2p_1$ states at impact energies 500, 400, and 300 eV. The absolute elastic differential cross sections $[d\sigma/d\Omega]_{\text{el}}$ are also listed. The square brackets denote powers of 10. The $[d\sigma/d\Omega]_{\text{el}}$ are obtained by the interpolation and extrapolation of the results of Bromberg [11] and Jansen *et al.* [12] and normalization to the zero-angle cross sections calculated by Byron *et al.* [13].

Angle (deg)	$[d\sigma/d\Omega]_{\text{el}}$ (a_0^2/sr)	Intensity ratio $1s_2$	$1s_4$	$2p_1$	$[d\sigma/d\Omega]_{\text{inel}}$ (a_0^2/sr) $1s_2$	$1s_4$	$2p_1$
			$E_i=500$ eV				
2.4	1.06[+1]	4.53[−1]	3.63[−2]	1.45[−2]	4.80	3.85[−1]	1.54[−1]
3.1	9.74	3.01[−1]	2.44[−2]	1.31[−2]	2.93	2.38]−1]	1.28[−1]

TABLE I. (*Continued*).

Angle (deg)	$[d\sigma/d\Omega]_{el}$ (a_0^2/sr)	Intensity ratio $1s_2$	Intensity ratio $1s_4$	Intensity ratio $2p_1$	$[d\sigma/d\Omega]_{inel}$ (a_0^2/sr) $1s_2$	$[d\sigma/d\Omega]_{inel}$ (a_0^2/sr) $1s_4$	$[d\sigma/d\Omega]_{inel}$ (a_0^2/sr) $2p_1$
3.7	9.07	2.15[−1]	1.71[−2]	1.16[−2]	1.95	1.55[−1]	1.05[−1]
4.2	8.56	1.72[−1]	1.35[−2]	1.14[−2]	1.47	1.15[−1]	9.75[−2]
4.7	8.09	1.25[−1]	9.55[−3]	1.16[−2]	1.01	7.73[−2]	9.35[−2]
5.2	7.65	9.79[−2]	7.61[−3]	1.07[−2]	7.49[−1]	5.83[−2]	8.15[−2]
6.2	6.87	5.80[−2]	4.60[−3]	9.06[−3]	3.98[−1]	3.16[−2]	6.22[−2]
7.2	6.18	3.29[−2]	2.46[−3]	7.05[−3]	2.03[−1]	1.52[−2]	4.35[−2]
8.2	5.57	1.93[−2]	1.02[−3]	5.25[−3]	1.08[−1]	5.70[−3]	2.93[−2]
9.2	5.03	1.27[−2]	7.57[−4]	3.93[−3]	6.40[−2]	3.81[−3]	1.98[−2]
10.2	4.55	5.62[−3]	4.63[−4]	3.02[−3]	2.55[−2]	2.10[−3]	1.37[−2]
12.2	3.70	1.65[−3]	1.56[−4]	1.43[−3]	6.11[−3]	5.76[−4]	5.30[−3]
15.6	2.56	1.03[−3]		9.58[−4]	2.65[−3]		2.46[−3]
17.6	2.06	1.57[−3]		9.10[−4]	3.24[−3]		1.87[−3]
20.6	1.47	1.90[−3]		1.40[−3]	2.80[−3]		2.06[−3]
23.6	1.06	1.83[−3]		2.58[−3]	1.93[−3]		2.73[−3]
26.6	7.77[−1]	1.24[−3]		2.10[−3]	9.63[−4]		1.63[−3]
			$E_i = 400$ eV				
2.4	1.13[1]	5.17[−1]	4.26[−2]	1.44[−2]	5.84	4.82[−1]	1.63[−1]
2.9	1.07[1]	3.95[−1]	3.13[−2]	1.38[−2]	4.22	3.34[−1]	1.48[−1]
3.3	1.02[1]	3.16[−1]	2.58[−2]	1.32[−2]	3.23	2.64[−1]	1.36[−1]
3.6	9.91	2.73[−1]	2.07[−2]	1.19[−2]	2.70	2.05[−1]	1.18[−1]
4.1	9.39	2.12[−1]	1.67[−2]	1.17[−2]	1.99	1.57[−1]	1.10[−1]
4.6	8.90	1.64[−1]	1.30[−2]	1.16[−2]	1.46	1.16[−1]	1.03[−1]
5.1	8.43	1.34[−1]	9.52[−3]	1.07[−2]	1.13	8.03[−2]	9.02[−2]
5.6	8.00	1.04[−1]	8.12[−3]	9.93[−3]	8.29[−1]	6.49[−2]	7.94[−2]
6.1	7.59	8.51[−2]	6.28[−3]	9.41[−3]	6.45[−1]	4.77[−2]	7.14[−2]
7.1	6.83	5.11[−2]	4.02[−3]	7.75[−3]	3.49[−1]	2.74[−2]	5.29[−2]
8.1	6.16	3.43[−2]	2.76[−3]	6.41[−3]	2.11[−1]	1.70[−2]	3.95[−2]
9.1	5.56	2.14[−2]	1.93[−3]	5.08[−3]	1.19[−1]	1.07[−2]	2.82[−2]
10.1	5.02	1.36[−2]	1.07[−3]	3.94[−3]	6.81[−2]	5.39[−3]	1.98[−2]
12.1	4.10	4.72[−3]	4.50[−4]	2.41[−3]	1.94[−2]	1.84[−3]	9.89[−3]
14.1	3.35	2.05[−3]	2.31[−4]	1.39[−3]	6.88[−3]	7.75[−4]	4.65[−3]
15.8	2.79	1.34[−3]		9.46[−4]	3.73[−3]		2.64[−3]
17.8	2.28	1.38[−3]		9.12[−4]	3.14[−3]		2.08[−3]
20.8	1.70	2.18[−3]		1.29[−3]	3.71[−3]		2.20[−3]
23.8	1.27	2.28[−3]		1.92[−3]	2.88[−3]		2.42[−3]
26.8	9.42[−1]	2.47[−3]		2.47[−3]	2.33[−3]		2.32[−3]
29.8	6.96[−1]	2.47[−3]		1.89[−3]	1.72[−3]		1.31[−3]
			$E_i = 300$ eV				
2.5	1.14[1]	5.73[−1]	4.56[−2]	1.43[−2]	6.54	5.20[−1]	1.63[−1]
3.0	1.08[1]	4.36[−1]	3.15[−2]	1.24[−2]	4.73	3.42[−1]	1.34[−1]
3.5	1.03[1]	3.48[−1]	2.71[−2]	1.23[−2]	3.58	2.79[−1]	1.27[−1]
4.0	9.79	2.80[−1]	2.11[−2]	1.14[−2]	2.75	2.06[−1]	1.12[−1]
5.0	8.87	1.87[−1]	1.28[−2]	1.04[−2]	1.66	1.14[−1]	9.21[−2]
6.0	8.05	1.23[−1]	9.55[−3]	9.59[−3]	9.89[−1]	7.69[−2]	7.72[−2]
7.0	7.32	8.34[−2]	6.22[−3]	8.99[−3]	6.10[−1]	4.55[−2]	6.58[−2]
8.0	6.66	5.67[−2]	4.33[−3]	7.39[−3]	3.78[−1]	2.88[−2]	4.92[−2]
9.0	6.07	3.92[−2]	2.78[−3]	5.96[−3]	2.38[−1]	1.69[−2]	3.62[−2]
10.0	5.53	2.58[−2]	2.01[−3]	4.70[−3]	1.42[−1]	1.11[−2]	2.60[−2]
12.0	4.59	1.26[−2]	9.28[−4]	3.05[−3]	5.77[−2]	4.26[−3]	1.40[−2]
13.7	3.90	5.80[−3]		2.13[−3]	2.26[−2]		8.29[−3]
15.7	3.23	2.26[−3]		1.27[−3]	7.29[−3]		4.10[−3]
18.7	2.44	1.63[−3]		8.83[−4]	3.98[−3]		2.15[−3]
21.7	1.84	2.32[−3]		1.09[−3]	4.27[−3]		2.01[−3]
24.7	1.40	2.94[−3]		1.72[−3]	4.10[−3]		2.40[−3]
27.7	1.06	3.05[−3]		2.41[−3]	3.25[−3]		2.56[−3]
30.7	8.17[−1]	3.49[−3]		2.68[−3]	2.85[−3]		2.19[−3]
33.7	6.33[−1]	3.14[−3]		2.68[−3]	1.99[−3]		1.70[−3]

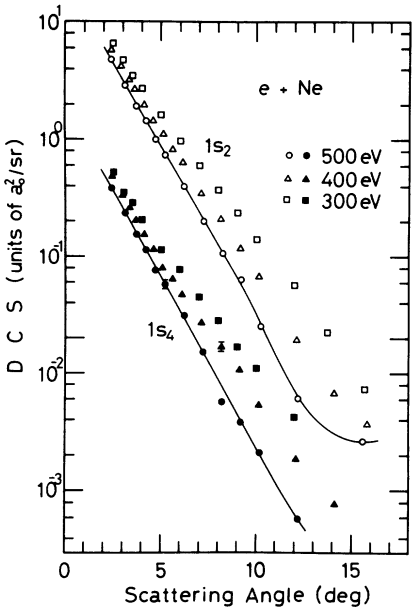

FIG. 2. Differential cross sections for the excitation of the $1s_2$ and $1s_4$ states in Ne as a function of the scattering angle in the range 2.5° to 15°.

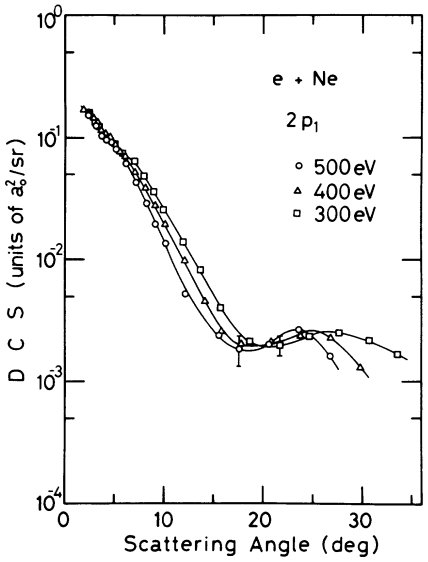

FIG. 4. Differential cross sections for the excitation of the $2p_1$ state in Ne as a function of the scattering angle from 2.4° to 30°.

about 15°. The DCS's for the $1s_2$ excitation are shown in Fig. 3 for the whole scattering angles measured. The DCS's for the $1s_2$ and $1s_4$ excitations have a steeply forward peaking angular dependence and those for the $1s_2$ excitation have the minima. It is found that the angle where the minimum appears becomes smaller as the impact energy is increased.

The DCS's for the $2p_1$ excitation are shown in Fig. 4 as a function of the scattering angle. It is found that the DCS's for the $2p_1$ excitation show a far more gentle angular dependence than those for $1s_2$ and $1s_4$ excitations. Besides, the impact energy dependence of the DCS's for the $2p_1$ excitation is relatively small and the DCS's for three different impact energies nearly overlap with one another at scattering angles smaller than 5°. The DCS's for the $2p_1$ excitation possess minima similar to those of the $1s_2$ excitation; however, the difference in the values of the DCS's at the minima is very small for the three different impact energies.

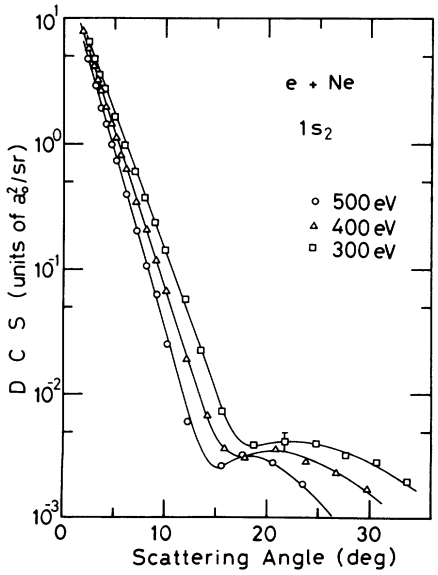

FIG. 3. Differential cross sections for the excitation of the $1s_2$ state in Ne as a function of the scattering angle from 2.5° to 30°.

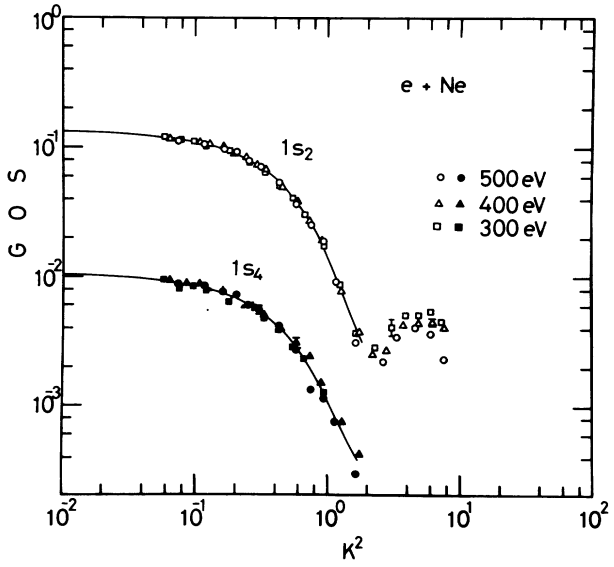

FIG. 5. The generalized oscillator strengths for the excitation of the $1s_2$ and $1s_4$ states in Ne as a function of the squared momentum transfer K^2 (log-log plots). The solid lines are fitted lines using Eq. (3).

TABLE II. Comparison of the present optical oscillator strengths for the $1s_2$ and $1s_4$ excitations in Ne with those of previous authors.

Author	OOS $1s_2$	OOS $1s_4$	Ratio OOS($1s_4$)/OOS($1s_2$)
EELS			
Present work	0.137±0.018	0.0106±0.0014	0.077
Geiger[a]	0.131±0.026	0.009±0.002	0.069
Brion[b]	0.153	0.0128	0.084
Optical measurements			
Tsurubuchi, Watanabe, and Arikawa[c]	0.123±0.006	0.0122±0.0006	0.099
Lawrence and Liszt[d]	0.130±0.013	0.0078±0.0004	0.06
Bhaskar and Lurio[e]	0.148±0.014	0.0122±0.0009	0.082
Calculations			
Albat and Gruen[f]	0.149	0.0113	0.076
Gold and Knox[g] (*A*)	0.110	0.011	0.1
(*B*)	0.121	0.012	0.099

[a]Reference [24].
[b]Reference [25].
[c]Reference [21].
[d]Reference [23].
[e]Reference [22].
[f]Reference [27].
[g]Reference [26]. Results (*A*) are based only on a wave function while (*B*) results from a semiempirical calculation.

The GOS's for the $1s_2$ and $1s_4$ excitations are computed from the DCS's using Eq. (2) and are shown in Fig. 5. The GOS's for the $2p_1$ excitation are also shown in Fig. 6. In the graph of the GOS against K^2, the data points for the $1s_2$ and $1s_4$ excitations taken at 300, 400, and 500 eV lie on the same curves in the region $K^2 < 1.5$. However, in the region $K^2 > 1.5$, where the GOS's for the $1s_2$ excitation have the minima and maxima, the GOS's show an impact-energy dependence. The GOS curve shows a minimum at around $K^2 = 2.5$ and increases again, forming a broad maximum at the K^2 value around 4. Apparent GOS's become larger as the impact energy decreases. The existence of the first minimum in the GOS curve for the excitation of the resonance lines in rare-gas atoms has already been reported in several papers [3,5,17,18]. In particular, Wong, Lee, and Bonham [19] reported the experimental value of the K^2 for the first minimum in the relative GOS for the $2p^5 3s$ transition at 25 keV impact energy. There is good agreement between their value, $K^2_{\min} = 2.66$, and the present value for the $1s_2$ transition, which is the dominant part of the $2p^5 3s$ transition, $K^2_{\min} \cong 2.5$.

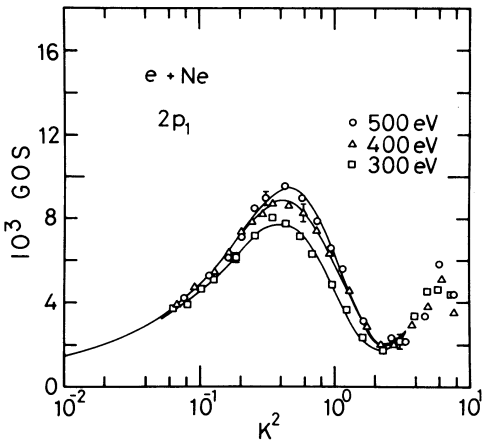

FIG. 6. The generalized oscillator strengths for the excitation of the $2p_1$ state in Ne as a function of the squared momentum transfer K^2 (semilog plots). The solid lines are fitted lines using Eq. (4).

As for the $2p_1$ excitation, the data points of the GOS's taken at 400 and 500 eV lie on the same curve in the regions, $K^2 \leq 0.2$ and $1 \leq K^2 \leq 2$. But in the other regions, the apparent GOS's depend on the impact energy. The GOS's taken at 300 eV are smaller than those at 400 and 500 eV over the whole range of K^2. It has been shown by Lassettre that the transition for which term symbols in the initial and final states are the same does not obey the Born approximation strictly, while the transitions for which the term symbol changes on excitation closely follow the Born approximation [20]. The $2p_1$ state is designated by the $^1S_0$ term, although the *LS* coupling notation does not perfectly designate the state. We suggest that these deviations from the Born approximation in the behavior of the GOS's for the $2p_1$ excitation at these high impact energies are attributable to its character of the *S* to *S* transition, where the term symbol does not change on the excitation process.

The present results of the OOS and the ratios of the

TABLE III. Integrated cross sections for the excitation of the $1s_2$ and $1s_4$ states in Ne.

Impact energy (eV)	Cross section (10^{-18} cm^2) $1s_2$	$1s_4$
300	4.88±0.63	0.383±0.050
400	4.04±0.53	0.317±0.041
500	3.47±0.45	0.272±0.035

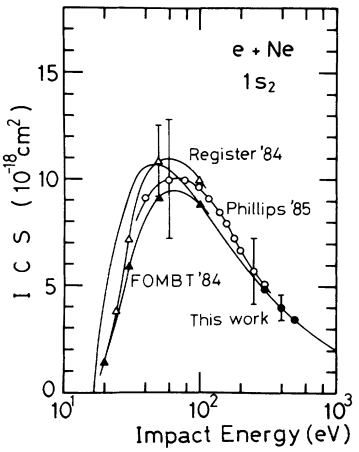

FIG. 7. Integrated cross sections for the excitation of the $1s_2$ state in Ne as a function of the impact energy. The solid circles are the present results and the solid curve is drawn by the extrapolation to the lower impact energies within the framework of the Born approximation using Eq. (5). The open circles are experimental results of Phillips, Anderson, and Lin (Ref. [8]); the open triangles are by Register *et al.* (Ref. [7]). The solid triangles are theoretical results of Machado, Leal, and Csanak calculated with FOMBT (Ref. [6]).

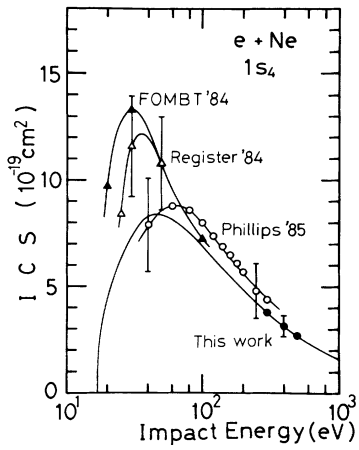

FIG. 8. Integrated cross sections for the excitation of the $1s_4$ state in Ne as a function of the impact energy. The same symbols and notations are used as in Fig. 7.

OOS for the $1s_4$ to the $1s_2$ are compared with other available data in Table II. The experimental absolute OOS are reported by Tsurubuchi, Watanabe, and Arikawa [21] using the self-absorption method, by Bhaskar and Lurio [22] using the cascade level crossing method, by Lawrence and Liszt [23] using the pulsed electron beam, and by Geiger [24] and Brion [25] using high-energy electron impact. The OOS's are also reported by Gold and Knox [26] using a calculation based only on a wave function (A) and a semiempirical calculation (B), and by Albat and Gruen [27] using a Hartree-Fock calculation with many configuration interactions.

The present result of the OOS for the $1s_2$ excitation is in good agreement with Lawrence and Liszt and Geiger. That for the $1s_4$ excitation agrees with Geiger, Gold and Knox, and Albat and Gruen. The ratios of the OOS for the $1s_4$ to the $1s_2$ agree well with the values of Geiger, Brion, and Albat and Gruen.

The ICS's for the $1s_2$ and $1s_4$ excitations at 300, 400, and 500 eV impact energies are determined using Eq. (5) and are tabulated in Table III. From the GOS's taken at 300, 400, and 500 eV, ICS's at lower impact energies can be calculated within the framework of the Born approximation. These results are shown in Figs. 7 and 8, where other values measured by Register *et al.* [7] and Phillips, Anderson, and Lin [8] and calculated by Machado, Leal, and Csanak [6] with the FOMBT, are also presented for comparison. The present ICS values for the $1s_2$ excitation agree very well with the values of Phillips, Anderson, and Lin at relatively high impact energies. At lower impact energies, the values of Register *et al.* and Phillips, Anderson, and Lin agree with the values of FOMBT within the experimental errors. Our ICS values for the $1s_4$ excitation also agree with the values of Phillips, Anderson, and Lin at relatively high impact energies. But at lower impact energies, the values of Phillips, Anderson, and Lin are not in good agreement with the values of Register *et al.* and Machado, Leal, and Csanak (FOMBT) in a shape of the curve.

The systematic errors in the measured DCS's due to the effect of the limited angular resolution are negligibly small in the present experiment. The errors in the results of the DCS's and GOS's are estimated to be 12%, as the quadratic sum of the random error, 9%, the systematic error, 3%, and the error of the standard elastic-scattering cross section, 8%. The uncertainties in the OOS are estimated to be 13% as the quadratic sum of the errors of the GOS's (12%) and the errors induced in the extrapolation procedure of the GOS's (5%). The errors in the ICS's are also of a similar extent.

[1] G. P. Li, T. Takayanagi, K. Wakiya, H. Suzuki, T. Ajiro, S. Yagi, S. S. Kano, and H. Takuma, Phys. Rev. A **38**, 1240 (1988).

[2] T. Takayanagi, G. P. Li, K. Wakiya, H. Suzuki, T. Ajiro, T. Inaba, S. S. Kano, and H. Takuma, Phys. Rev. A **41**, 5948 (1990).

[3] T. Y. Suzuki, Y. Sakai, B. S. Min, T. Takayanagi, K. Wakiya, H. Suzuki, T. Inaba, and H. Takuma, Phys. Rev. A **43**, 5867 (1991).

[4] P. S. Ganas and A. E. S. Green, Phys. Rev. A **4**, 182 (1971).

[5] T. Sawada, J. E. Purcell, and A. E. S. Green, Phys. Rev. A **4**, 193 (1971).

[6] L. E. Machado, E. P. Leal, and G. Csanak, Phys. Rev. A **29**, 1811 (1984).

[7] D. F. Register, S. Trajmar, G. Steffensen, and D. C. Cart-

wright, Phys. Rev. A **29**, 1793 (1984).
[8] M. H. Phillips, L. W. Anderson, and C. C. Lin, Phys. Rev. A **32**, 2117 (1985).
[9] M. Shaw, M. J. G. Borge, and J. Campos, J. Chem. Phys. **80**, 1882 (1984).
[10] C. E. Moore, *Atomic Energy Levels,* Natl. Bur. Stand. (U.S.) Circ. No. 467 (U.S. GPO, Washington, D.C., 1958), Vol. I.
[11] J. P. Bromberg, J. Chem. Phys. **61**, 963 (1974).
[12] R. H. J. Jansen, F. J. de Heer, H. J. Luyken, B. van Wingerden, and H. J. Blaauw, J. Phys. B **9**, 185 (1976).
[13] F. W. Byron, Jr. and C. J. Joachain, Phys. Rev. A **15**, 128 (1977).
[14] H. Bethe, Ann. Phys. (Leipzig) **5**, 325 (1930).
[15] K. N. Klump and E. N. Lassettre, J. Chem. Phys. **68**, 886 (1978).
[16] M. A. Dillon and E. N. Lassettre, J. Chem. Phys. **62**, 2373 (1975).
[17] Y. K. Kim, M. Inokuti, G. E. Chamberlain, and S. R. Mielczarek, Phys. Rev. Lett. **21**, 1146 (1968).
[18] P. G. Burke, A. Hibbert, and W. D. Robb, J. Phys. B **4**, 153 (1971).
[19] T. C. Wong, J. S. Lee, and R. A. Bonham, Phys. Rev. A **11**, 1963 (1975).
[20] E. N. Lassettre, J. Chem. Phys. **53**, 3801 (1970).
[21] S. Tsurubuchi, K. Watanabe, and T. Arikawa, J. Phys. Soc. Jpn. **59**, 497 (1990).
[22] N. D. Bhaskar and A. Lurio, Phys. Rev. A **13**, 1484 (1976).
[23] G. Lawrence and H. S. Liszt, Phys. Rev. **178**, 122 (1969).
[24] J. Geiger, Phys. Lett. A **33**, 351 (1970).
[25] C. E. Brion (private communication).
[26] A. Gold and R. S. Knox, Phys. Rev. **113**, 834 (1959).
[27] R. Albat and N. Gruen, J. Phys. B **7**, L9 (1974).